INT. J. REMOTE SENSING, 20 JULY, 2004,
VOL. 25, NO. 14, 2725–2745

Taylor & Francis
Taylor & Francis Group

Modelling the reflectance anisotropy of Chihuahuan Desert grass–shrub transition canopy–soil complexes

M. J. CHOPPING*
Earth and Environmental Studies, Montclair State University, Upper Montclair, NJ 07043, USA

L. H. SU
Research Centre for Remote Sensing, Beijing Normal University, Beijing 100875, PR China

A. RANGO and C. MAXWELL
USDA, ARS Jornada Experimental Range, Las Cruces, NM 88003, USA

(*Received 10 December 2002; in final form 11 July 2003*)

Abstract. The goal of the research presented here is to assess the factors controlling the remotely sensed signal returned in the solar wavelengths from Chihuahuan Desert grass–shrub transition canopy–soil complexes. The specific objectives were twofold: to evaluate the importance of the different elements (overstorey, understorey, soil) in the bidirectional reflectance distribution function (BRDF) of a Chihuahuan Desert grass–shrub transition zone; and to explore the behaviour of simple parametric and explicit scattering models with respect to observations. The first objective was approached by simulations using the Radiosity Graphics Method (RGM), with surface parameters provided by measurements of plant locations and dimensions obtained over two contrasting 25 m^2 plots. The second was approached through simulations of bidirectional reflectance factors (BRFs) by both the RGM and a Simplified Geometric Model (SGM) developed for inversion purposes. The modelled BRFs were assessed against multi-angle observations (MAO) – samples of the BRDF at a wavelength of 650 nm acquired from the air at up to six view zenith angles and three solar zenith angles. The results show that the understorey of small forbs and sub-shrubs plays an important role in determining the brightness and reflectance anisotropy of grass–shrub transition landscapes in relation to that of larger shrubs such as mesquite and ephedra. This is owing to the potentially high density of these plants and to the fact that there is also a varying proportion of black grama grass and prone grass litter associated with snakeweed abundance. Both of these components darken the scene. The SGM performed well measured against both the RGM and the MAO at the MAO acquisition angles (R^2 of 0.98 and 0.92, respectively) and good correlations were obtained between RGM and SGM when modelling was performed at a wider range of angular configurations ($R^2 \approx 0.90$). The SGM was shown to be highly sensitive to its adjustable parameters. Both models underestimated BRF magnitude with respect to the MAO by a small amount (< 6%), showing increasing divergence from the backscattering into the forward-scattering direction. A remaining problem for operational model inversions using MAO is the *a priori* estimation of understorey and grass abundance.

*Corresponding author; e-mail: choppingm@mail.montclair.edu

International Journal of Remote Sensing
ISSN 0143-1161 print/ISSN 1366-5901 online © 2004 Taylor & Francis Ltd
http://www.tandf.co.uk/journals
DOI: 10.1080/01431160310001618437

1. Introduction

Obtaining information on the physical structure and biophysical characteristics of terrestrial surfaces over large areas remotely has long been the goal of satellite Earth observation programmes, with a broad potential for applications at a global scale (Hall *et al.* 1995). For passive sensors which detect and quantify the spectral radiance reflected by the Earth's surface in the solar wavelengths (0.4–1.0 μm), retrieval of this surface information is complicated by atmospheric scattering, absorption and reflectance by aerosols and gases and by the nature of interactions with surface elements, particularly with respect to the angular distribution of outgoing radiance in relation to the direction of illumination, described by the bidirectional reflectance distribution function (BRDF). For some terrestrial surfaces, the BRDF can be described using radiative transfer (RT) plane-parallel or turbid medium models which are well adapted for horizontally semi-infinite canopies such as arable crops with high fractional vegetation cover and a homogeneous (uniform) spatial distribution. With such models and suitable multi-angular reflectance datasets it is possible to retrieve surface information unavailable in the nadir-spectral domain, such as canopy height and 3D structure, as well as information on canopy biochemistry (Verstraete *et al.* 1990, Asner *et al.* 1999). However, for arid and semi-arid environments the assumption of uniformity does not hold because vegetation is highly clumped and patchy and, for these canopies, geometric-optical (GO) or hybrid geometric-optics/radiative transfer (GORT) models are more appropriate (Ni and Li 2000). The grass–shrub transition zones of the Chihuahuan Desert in southern New Mexico are in this category. These zones exist at the boundary of change, where grassland is giving way to shrubland as a result of a number of processes, of which anthropogenic disturbance in the latter part of the last century in the form of overgrazing and climate change are the most important (Smith *et al.* 2000). There is considerable interest in the direction of change at transition zone sites as these ecotones are more sensitive to both disturbance and climate change than either grasslands or well-developed shrublands (Friedel 1991, Archer *et al.* 2001, Smith *et al.* 2000). Radiosity methods are also appropriate as these model canopy physical structures explicitly and rely on fewer and less important approximations and assumptions than RT or GORT models (Goel 1988, Wernecke *et al.* 2000). In particular, they are able to consider all orders of scattering with scene elements (Qin and Gerstl 2000).

Both GORT and radiosity BRDF modelling approaches to the BRDFs of Chihuahuan Desert transition zones have been shown to give reasonable results and both have been validated against POLDER and Advanced Very High Resolution Radiometer (AVHRR) satellite observations at specific view-illumination combinations (Ni and Li 2000, Qin and Gerstl 2000). However, these validation efforts were hampered by the very large footprints of the satellite-borne sensors (6–8 km and 1.1–4 km, respectively) in relation to the spatial variability of surface parameters; by the lack of a detailed and accurate specification of plant locations and dimensions; and because the models are not easily invertible for the parameters of interest (canopy height, shrub density, shrub size distribution, leaf area index (LAI)). To address these concerns a multiple view angle (MVA) reflectance dataset for the end of the wet season (September) was obtained from an airborne platform (the USDA, ARS Cessna Twin 404); a detailed, accurate map of plant locations and dimensions was compiled; and a simplified geometric-optics model (SGM) was developed and validated (Chopping *et al.* 2003).

The goal of the research presented here is to promote understanding of the

factors controlling the remotely sensed signal returned in the solar wavelengths from Chihuahuan Desert grass–shrub transition canopy–soil complexes, particularly with respect to reflectance anisotropy. The first objective was to use simulations to evaluate the importance of the different elements (overstorey, understorey, soil) in the BRDF of a Chihuahuan Desert grass–shrub transition zone by simulations using radiosity methods together with detailed measurements of plant locations and dimensions surveyed over an area comparable to the intrinsic length scale of the albedo of the landscape (ca 33 m; Pelgrum *et al.* 2000). The second objective was to explore the behaviour of both simple parametric and explicit scattering models with respect to observations and to each other.

2. Site description

The USDA, ARS Jornada Experimental Range (JER) covers 783 km^2 and lies 37 km north of Las Cruces in southern New Mexico in the northern part of the Chihuahuan Desert. It is located between the Rio Grande floodplain (elevation 1186 m) on the west and the crest of the San Andres mountains (2833 m) on the east (figure 1). Vegetation on the JER is usually classified as desert grassland but shrub density has not only increased in the past but is continuing to do so (Gibbens *et al.* 1992). Mesquite (*Prosopis glandulosa* Torr.) is now a major dominant on sandy soils

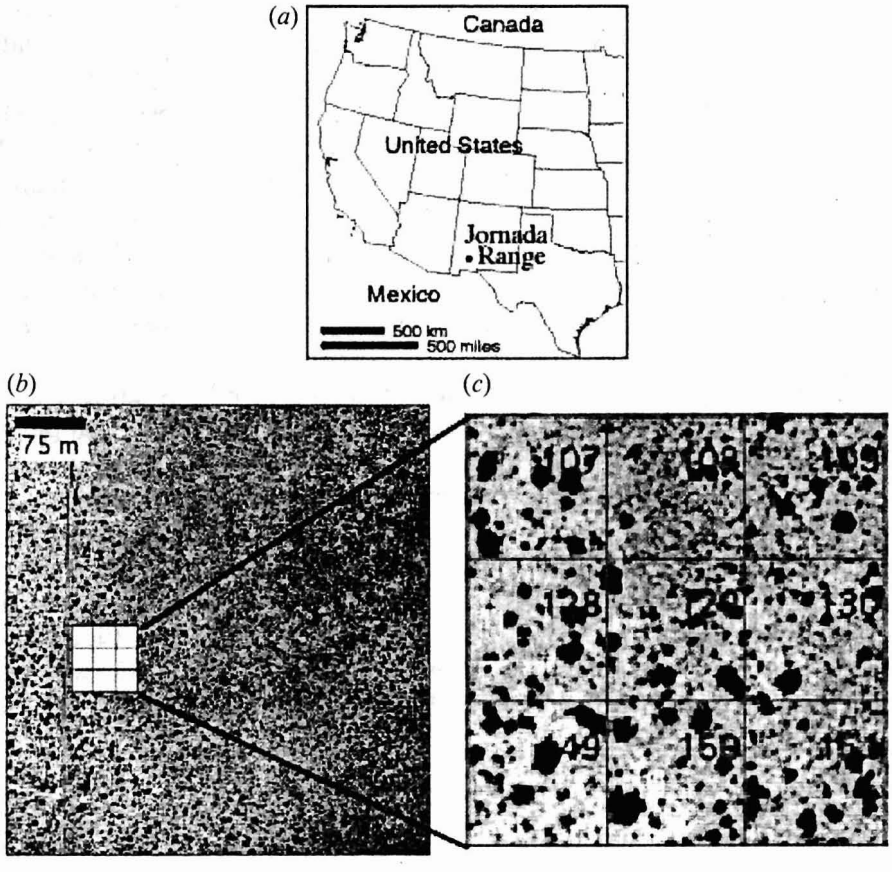

Figure 1. (*a*) Location of the Jornada Experimental Range; (*b*) transition zone aerial photograph; (*c*) transition zone aerial photograph chip 3 × 3 grid of 25 m^2 plots (numbered). The large dark objects are honey mesquite shrubs. Mottled, darker areas have a higher snakeweed density.

where broom snakeweed (*Gutierrezia sarothrae*) and soaptree yucca (*Yucca elata*) are also abundant (figure 1(*c*)). The observed changes in the spatial distribution of vegetation and soil resources corresponds with what is called the 'Jornada desertification model' which states that sustained increased pressure ultimately results in the spatial redistribution of soil resources and especially nutrients towards a more clumped, woody canopy with larger exposed soil patches in inter-shrub spaces. This model is built on observations of grassland to woodland transitions in arid regions around the world (Schlesinger *et al.* 1990) and is particularly appropriate here. Since the middle of the last century there has been a rapid conversion of native C_4 grasslands to C_3 shrublands in many parts of the southwest USA and this is reflected in transitions at the JER: in the area covered by vegetation surveys (585 km^2) 388 km^2 or 58% was native grassland with no shrubs (mesquite, tarbush, or creosote bush) (Buffington and Herbel 1965) in 1858 but by 1963 there was very little native grassland completely free of shrubs. In spite of the differences in structure, the grassland and transition shrubland sites do not differ greatly in terms of aboveground primary production (Huenneke *et al.* 2002), which is limited by moisture and nutrient availability.

Since 1995 USDA, ARS scientists have increased efforts to use remote sensing techniques to study changes in the vegetation of the JER. In particular, the USDA, ARS Hydrology & Remote Sensing Laboratory initiated a series of biannual field campaigns, the JORNada EXperiment (JORNEX), to provide ground data in support of satellite and aircraft observations (Ritchie *et al.* 1996). JORNEX initially focused on three important Chihuahuan desert landscape types: black grama grassland, grass–shrub transition and honey mesquite coppice dunes and, in 2000, was extended to include a tarbush community. The transition site (figure 1(*c*); figure 2) exhibits transitional vegetation dynamics characteristic of the northern Chihuahuan Desert. In 1915 three awn – a short-lived perennial grass species – dominated the transition study area but it is now largely dominated by mesquite and it is expected that the transition site will undergo further vegetation change towards shrub domination over the next few decades.

Vegetation at the site differs importantly from the JORNEX grass and dune shrubland sites in many respects and particularly in the 'clumpiness' or 'gappiness' of the canopy, with the grass site the most spatially continuous (homogeneous) and the mesquite dune site the most spatially discontinuous (heterogeneous): the transition site is between the two and is usually regarded as an ecotone. Field photography at low sun elevations provides an indication of the importance of geometric effects: in the solar direction (forward-scattering), shadows cast by the plants are clearly visible while, in the anti-solar (backscattering) direction, shadows are largely hidden (figure 2). The transition site also represents the most complex of canopy types in the JER with respect to architecture, both horizontally and vertically (figure 3).

3. Methods

3.1. *Vegetation mapping*

The targets are two 25 m^2 plots close to the JORNEX transition site. The canopy–soil complex may be considered to be composed of three levels:

1. overstorey: large and medium-sized shrubs; mainly mesquite, acacia, ephedra and yucca;
2. understorey: mainly snakeweed with some small shrubs and grasses;
3. bare soil: mostly without crusts, rather sandy in texture but also some silt.

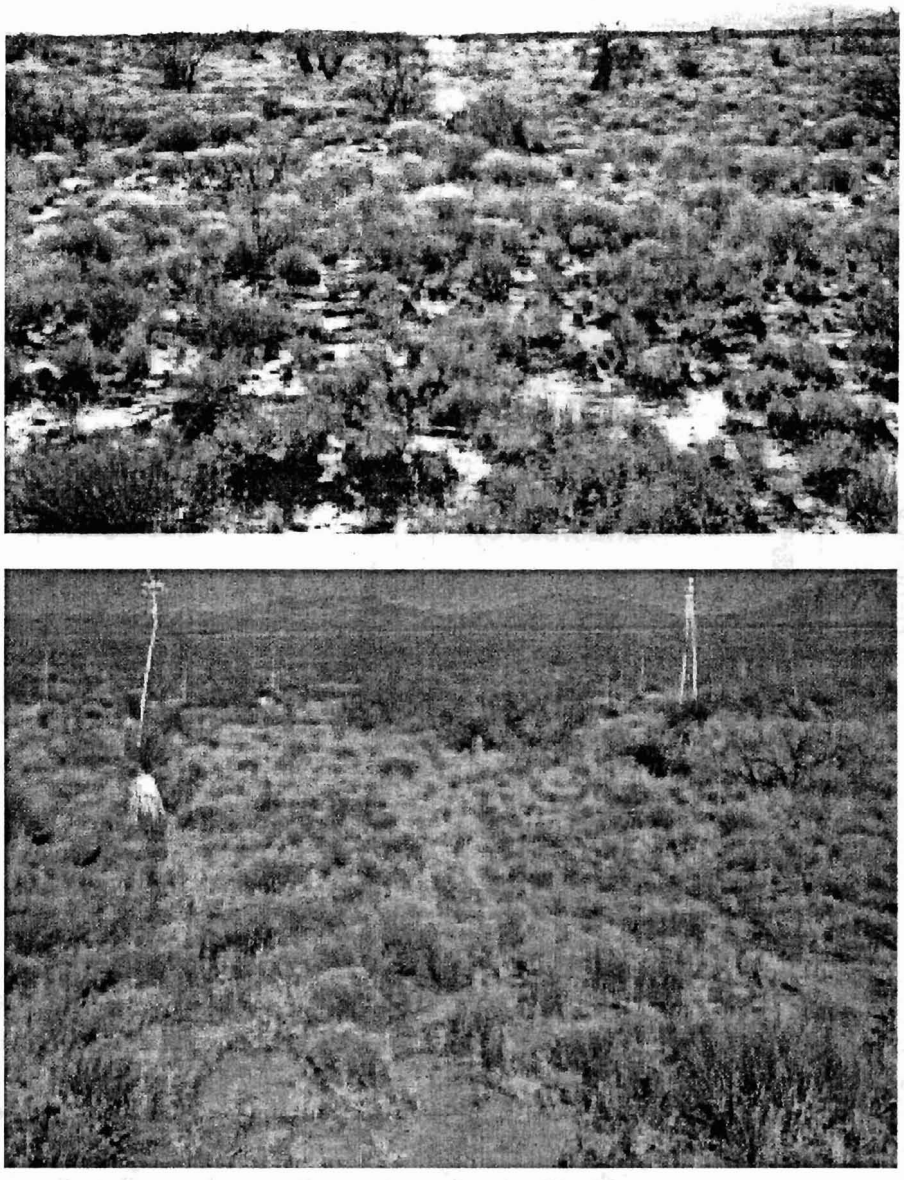

Figure 2. Ground view in the principal plane with a high solar zenith angle at ca 5:00 p.m. on 25 January 2002: (*a*) forward scattering; (*b*) backscattering. Notice the darkening effect of shadowing in the former and the differing apparent soil brightness and colour.

A digital scan of a high-resolution aerial photograph was used to identify and locate the larger plants which make up the overstorey. The flights took place on 27 September 1999 at an altitude of 2500 m above sea level (about 1200 m above ground level) between 1700 and 1800 GMT with solar zenith angles of 40–43°. The mapping camera was a Leica Wild RC-30 with 6-inch focal length and using Kodak SO-134 Aerochrome Infrared film sensitive in the wavelength region 510–900 nm. An image from a 9 × 9 inch positive acquired over the JORNEX transition site was scanned and resampled to a Universal Transverse Mercator (UTM) map projection on a grid with a 25 cm interval, comparable to the intrinsic resolution of the photography. Simple thresholding was used to identify large plants and prints for

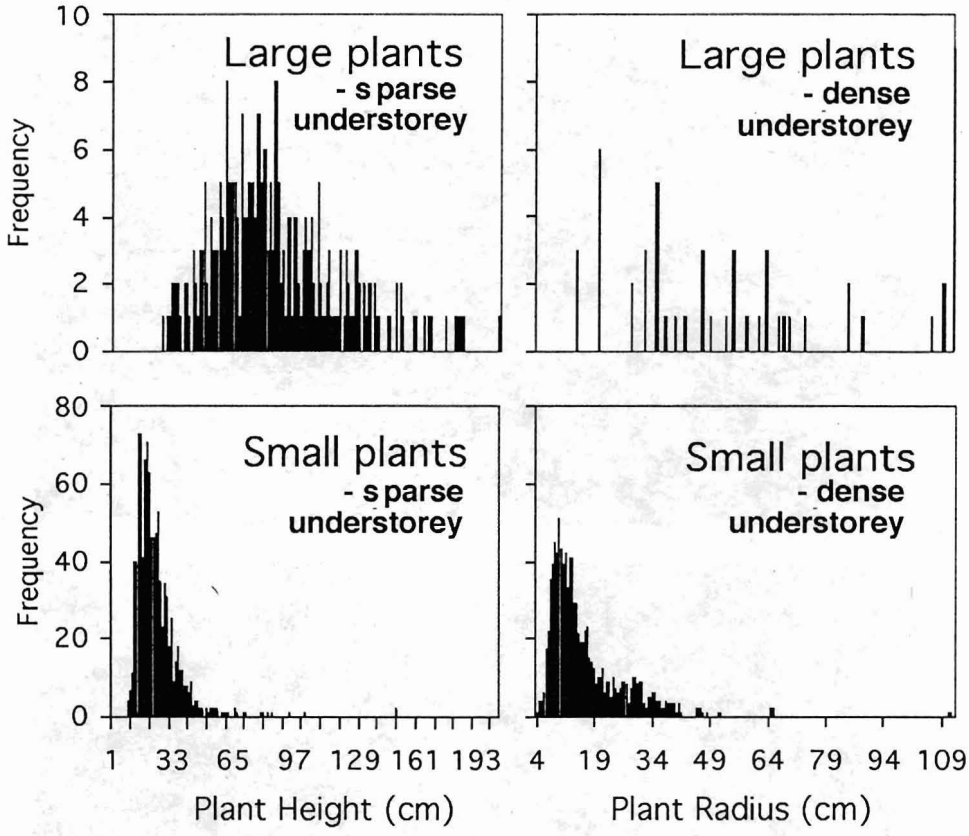

Figure 3. Frequency distribution for large and small plant heights and radii surveyed in two contrasting (sparse and dense understorey) 25 m^2 plots.

each of the 25 m^2 plots in the 3 × 3-plot target area. Clumps of several yucca crowns and very large and flourishing Mormon tea (*Ephedra torreyana*) appear in the thresholded aerial image. Fieldwork was carried out to locate, identify and measure the heights of all plants appearing in the image. Two sets of measurements for each 25 m^2 plot were made: (i) the heights and species of all large plants appearing on the large plant coverage from a thresholded aerial photograph were noted; (ii) small plant type, dimensions (height, major axis) and location within 1 m quadrats were acquired by transcription onto sets of five sheets marked with 5 × 5 × 1 m grids.

In order to map the precise locations (± 10 cm) of all plants not appearing in the large plant maps (i.e. 'small plants'), meticulous field survey was carried out along 1 m wide corridors for two plots representing the extremes in small plant density: #107 (sparse) and #108 (dense). These plot numbers refer to the locations in figure 1(*c*). The vast majority (99.9%) of small plants surveyed were snakeweed, with some small Mormon tea, yucca and honey mesquite (table 1). Each corridor was surveyed in 1 m quadrats with the data collated into 25 m^2 images to cover a plot. Height and length of major axis were recorded for all plants except black grama grass (*Bouteloua eriopoda*), which accounted for a very small proportion of total cover.

The small plant location, type and dimensions data were digitized and combined with the large plant maps to form a detailed plant map for the two surveyed plots. To our knowledge this is the first time that such a detailed survey with explicit spatial and structural information has been acquired over

Table 1. Number and mean height, radius, area and perimeter of common plants in the JORNEX grass–shrubland transition zone.

			Means (m or m^2)				
Common name	Species	Abbreviation	Count	Radius	Height	Area	Perimeter
Broom snakeweed	*Gutierrezia sarothrae*	GUSA	1007	0.16	0.23	0.10	1.00
Honey mesquite	*Prosopis glandulosa*	PRGL	232	0.75	0.79	2.63	6.87
Mormon tea	*Ephedra torreyana*	EPTO	18	0.43	0.79	0.75	3.31
Soaptree yucca	*Yucca elata*	YUEL	58	0.32	0.84	0.39	2.50

Sample area 1250 m^2

this site. The raster (spatial, locational) and attribute (species, height, radius) data for both large and small plants were combined to produce vector maps of plant cover in which a unique code identifies each plant, relating it to an attribute table.

3.2. *Remotely sensed multi-angle observations (MAO)*

Remotely sensed multi-angle observations (MAO) must be acquired from the air or from space because of the long intrinsic length scales of the canopy–soil complex (Pelgrum *et al.* 2000). Multi-angle images were acquired from the air as part of the end of wet season JORNEX campaign of September 2000 (Chopping *et al.* 2003). The DuncanTech camera (Model: MS21003) used to collect the imagery is a 3-CCD progressive scan digital camera using a colour-separating prism, trim filters and three sensors to provide multi-spectral images in three channels. In this instance the camera was operated in CIR (colour-infrared) mode with green, red and near-infrared channels centred on 500 nm, 650 nm and 800 nm with bandpasses of 70 nm, 40 nm and 65 nm, respectively. The images produced by the CCDs are 656 cells in X by 493 cells in Y. The main lens is a 17 mm Tokina with a fixed focal length, f3.5 fixed and designed for 35 mm film but only the 6.4 mm × 4.8 mm central portion of the instantaneous field-of-view (IFOV) is used, minimizing distortion, radial drop-off in luminosity and vignetting. The camera thus has a 22° total field-of-view. Variable viewing zeniths were obtained by mounting the camera on a tilting bracket and adjusting the tilt along the flightline so that the view zenith angles near the centre of the target are −35°, −20°, 0° (nadir), +20°, +25° and +30° (example values are −34°, −20°, −6°, +22°, +26°, +31°), where by convention negative values indicate the backscattering hemisphere and positive values indicate the forward-scattering hemisphere (figure 4). The observations mostly lie close to the principal plane (PP) with a rather small offset. The ground-projected IFOVs (GIFOVs) of the MAO were between ca 1.5 and ca 2.0 m but the images were convolved with a pseudo-Gaussian point spread function in order to simulate the response of a sensor with a 50 m GIFOV and were subsequently sampled at a 25 m interval to obtain a smoother image. Surface reflectance values at 650 nm (red wavelength) were obtained by applying laboratory calibration coefficients for spectral radiance using the 6S code (v4.2; Vermote *et al.* 1997) with estimates of the condition of the atmosphere at the time of the overflights. Only 650 nm reflectance data were used because the contrast between vegetation and soil is greatest in this region. The results were checked by reference to ground radiometry over 8 m^2 tarps of known spectral reflectance which appeared in the MAO images (Chopping *et al.* 2003).

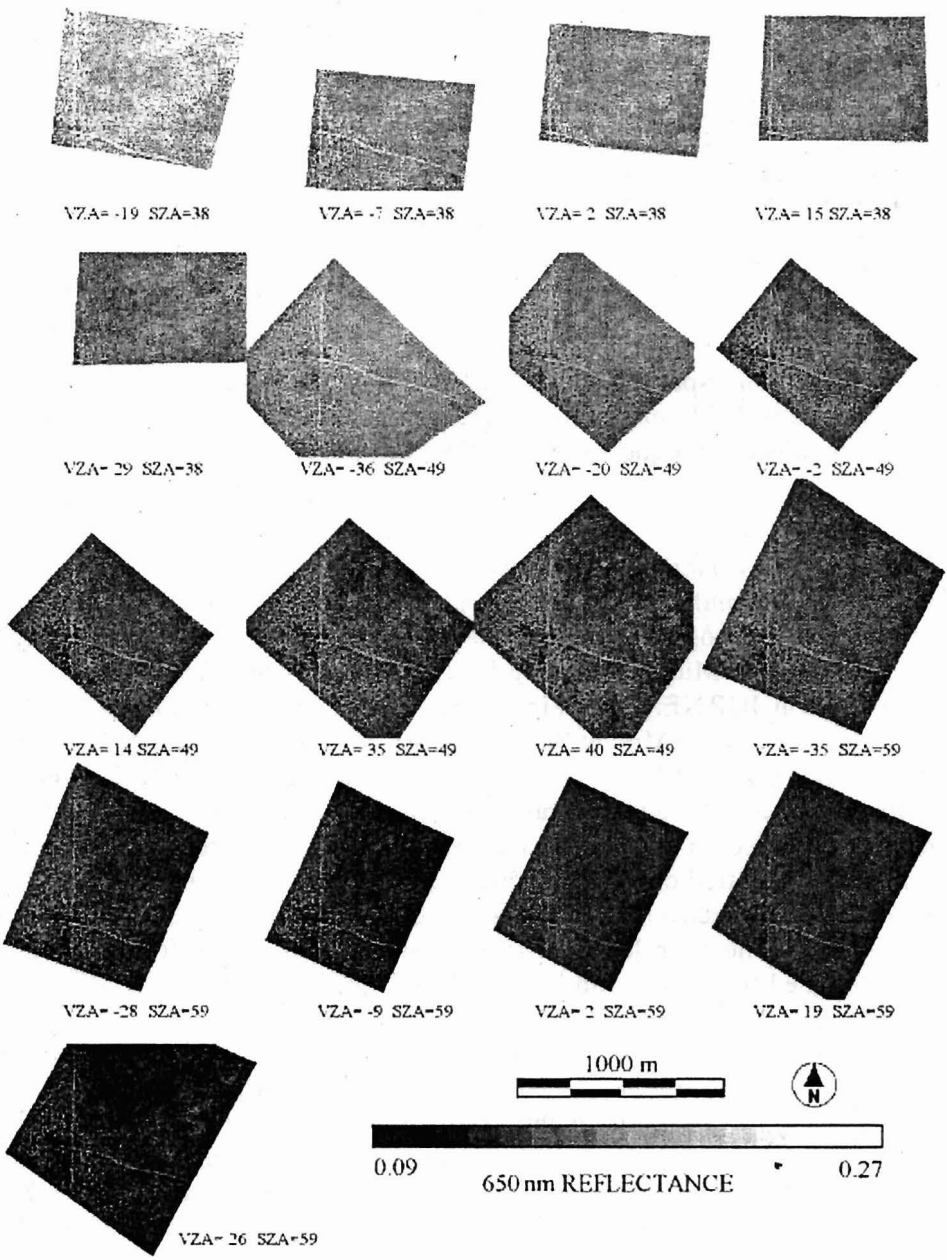

Figure 4. Multi-angle bidirectional reflectance images over the JORNEX transition site, aligned so that each row (column) has the same latitude (longitude). VZA, view zenith angle; SZA, solar zenith angle. Angles given are for the target centres. Negation indicates backscattering.

3.3. *BRDF modelling*

3.3.1. *Radiosity Graphics method (RGM)*

The RGM is a 3D scene modelling package capable of using plant architectures modelled with L-systems codes together with radiosity techniques. Radiosity is based on scene geometry alone rather than on particular viewing/illumination sampling régimes: all energy emitted or reflected by every surface in a scene is accounted for by its reflection and absorption by other surfaces. Radiosity methods

Table 2. Spectral reflectance values at 650 nm used in the BRDF modelling.

Component name	Spectral reflectance (650 nm)	Source
Bare soil	0.245	JORNEX
Honey mesquite leaf	0.095	PROVE*
Honey mesquite stem	0.075	PROVE
Soaptree yucca leaf	0.095	PROVE
Soaptree yucca stem	0.140	PROVE
Broom snakeweed	0.110	JORNEX
Mormon tea	0.200	JORNEX
Undergrowth†	0.050	estimated

*NASA EOS Grassland Prototype Validation Experiment (PROVE), May–June 1997.
†Estimated and used in SGM simulations only. JORNEX values derived from reflectance spectra.

thus calculate the radiation regime within 3D structures and allow the calculation of bidirectional reflectance, albedo and fraction of absorbed photosynthetically active radiation (*f*APAR). They are able to compute the proportions of an instrument IFOV which are filled with sunlit and shaded instances of the various surface components (shrub leaves, shrub stems and soil). Here, the RGM was driven using the database of plant locations, types and dimensions for the two surveyed plots. Optical properties of the different plant and soil components were obtained from the literature (Everitt *et al.* 1997, Asner *et al.* 2000, White *et al.* 2000) and from JORNEX reflectance spectra measurements (table 2). An empirical soil BRDF derived from field goniometry was used to evaluate the contribution from illuminated soil, rather than treating this as a Lambertian surface. The assumption of rather low diffuse (skylight) to direct irradiance conditions was made (1 : 12) – in the middle range of estimates for these wavelengths – and this was factored into calculations of total spectral reflectance for the proportions of shaded components. Leaf:stem ratios of 10 : 1, 8 : 1 and 3 : 1 were adopted for mesquite, ephedra and yucca, respectively. Measured leaf:stem ratios are somewhat lower than this (White *et al.* 2000) but were for end of dry season (May) rather than end of wet season (September) and do not include intra-shrub shadowing. The values used are, therefore, best estimates based on observed bulk reflectance of large shrubs.

Since the MAO were acquired at three solar zenith angles (SZA), it is interesting to evaluate the different probabilities of viewing the two major sunlit and shaded components (plant crowns and soil) under these illumination conditions. Calculations using the plant/soil data with the RGM showed that sunlit soil makes by far the most important contribution, up to 83% at lower sun elevations from a minimum of 73% at the highest sun elevation (table 3). Sunlit vegetation as a whole makes a maximum of only 11% of the total contribution from sunlit components, accounted for mainly by snakeweed and mesquite. Yucca and ephedra make up only 0.4% combined, almost all of which is accounted for by yucca. To provide an indication of the relative importance of the understorey the RGM was also run with all snakeweed 'removed', i.e. with the proportions of sunlit and shaded snakeweed and soil shaded by snakeweed re-assigned to sunlit soil, effected by applying a scaling coefficient based on the proportions of soil illuminated with and without the snakeweed calculated using Boolean geometry and the field measurements.

Table 3. Proportions of the components at different sun-view geometries (plot 107; sparse understorey).

Geometry (°)			Proportions (%)									
			Sunlit					Shaded				
SZA	VZA	RAA	soil	GUSA	PRGL	YUEL	EPTO	soil	GUSA	PRGL	YUEL	EPTO
37.5	20.5	21.0	82.5	4.8	4.4	0.3	0.0	2.1	5.3	0.5	0.1	0.0
37.5	8.3	31.5	82.6	3.3	3.8	0.3	0.0	3.1	6.1	0.6	0.1	0.0
37.5	4.3	48.8	82.5	3.1	3.7	0.3	0.0	3.4	6.1	0.7	0.1	0.0
37.5	14.1	175.1	81.5	2.0	3.2	0.2	0.0	3.6	7.8	1.5	0.2	0.0
37.5	27.4	170.0	79.9	1.6	2.9	0.2	0.0	4.0	8.9	2.2	0.3	0.0
49.0	35.2	6.0	80.1	5.6	5.0	0.4	0.0	3.0	5.3	0.4	0.1	0.0
49.0	19.6	9.6	80.0	4.4	4.1	0.3	0.0	4.7	5.7	0.8	0.1	0.0
49.0	1.3	124.8	80.2	2.2	3.0	0.2	0.0	6.0	6.9	1.3	0.2	0.0
49.0	14.0	176.6	78.9	1.7	2.6	0.2	0.0	6.2	8.1	2.1	0.2	0.0
49.0	34.7	173.9	76.4	1.1	2.1	0.1	0.0	6.7	9.9	3.3	0.4	0.1
49.0	40.2	173.8	75.3	1.0	2.0	0.1	0.0	6.7	10.6	3.8	0.4	0.1
59.3	36.3	7.9	75.7	5.4	5.0	0.3	0.0	7.3	5.6	0.5	0.1	0.0
59.3	29.6	7.0	75.6	4.8	4.5	0.3	0.0	8.2	5.7	0.6	0.1	0.0
59.3	11.7	1.7	75.1	2.9	3.5	0.2	0.0	10.3	6.7	1.0	0.2	0.0
59.3	3.1	26.1	75.0	2.5	3.1	0.2	0.0	11.1	6.7	1.2	0.2	0.0
59.3	16.7	161.7	73.9	1.5	2.5	0.1	0.0	10.9	8.5	2.3	0.3	0.0
59.3	23.6	162.9	73.2	1.3	2.3	0.1	0.0	11.0	9.1	2.7	0.3	0.0

Note: SZA, VZA are solar and view zenith angles, respectively; RAA is relative azimuth angle calculated as |SZA–VZA| if |SZA–VZA| <180, else $360 - |SZA–VZA|$. See table 1 for species abbreviations.

3.3.2. *Simple geometric model (SGM)*

The SGM (Chopping *et al.* 2003) was derived using the principles of Boolean geometry and volume scattering developed by Li and Strahler (1992) and Ross (1981), with further developments by Roujean *et al.* (1992) and Wanner *et al.* (1995). The model is designed to account for large-scale geometrical effects (protrusion density, shape and height of objects), for the spectral–directional properties of the soil/litter background, and for volume-scattering effects within crowns. The model formulation is shown in equation (1):

$$R = G_{\text{Walthall}}(\theta_i, \theta_v, \varphi)k_G(\theta_i, \theta_v, \varphi) + C_{\text{Ross}}(\theta_i, \theta_v, \varphi)k_C(\theta_i, \theta_v, \varphi) \quad (1)$$

where θ_i, θ_v and θ are the view zenith, solar zenith and relative azimuth angles, respectively; k_G and k_C are the calculated proportions of sunlit and viewed background and crown, respectively; G_{Walthall} is the Walthall model (Walthall *et al.* 1985) adjusted against field goniometer data; and C_{Ross} is the simplified Ross turbid medium approximation for optically-thin or thick plane parallel canopies (Ross 1981). k_G and k_C are calculated exactly via Boolean geometry for the principal (PP) and perpendicular (CPP) planes and approximated away from these; they are provided by equations (2) and (3), respectively.

$$k_G = e^{-\lambda\pi r^2\{\sec\theta_i' + \sec\theta_v' - O(\theta_i, \theta_v, \varphi)\}} \quad (2)$$

$$k_C = \left(1 - e^{-\lambda\pi r^2 \sec\theta_v'}\right)\frac{1}{2}(1 + \cos\varepsilon') \quad (3)$$

where λ is the number density of objects; r is the average radius of these objects; O

is the overlap area between the shadows of illumination and viewing. These functions include the parameters *b/r* (vertical crown radius/horizontal crown radius) and *h/b* (height of crown centre/vertical crown radius) which describe the shape and height of the crown. The prime indicates equivalent zenith angles obtained by a vertical scale transformation in order to treat spheroids as spheres ($\theta' = \tan^{-1}(b/r \tan\theta)$; see Wanner *et al.* 1995). ε is the scattering phase angle given by equation (4):

$$\cos\varepsilon = \cos\theta_i \cos\theta_v + \sin\theta_i \sin\theta_v \cos\varphi \tag{4}$$

Green leaf reflectance at 650 nm is set to 0.09 (Everitt *et al.* 1997, Asner *et al.* 2000); this enters into the calculation of the contribution from volume scattering, which is determined by the simplified Ross turbid medium approximation for optically-thin or thick plane parallel canopies (Ross 1981). Ross' formula was simplified by both Roujean *et al.* (1992) and Wanner *et al.* (1995) to obtain the following function as an initial step in the derivation of model kernels equations (5) and (6):

$$C_{\text{Ross}} = \frac{4\rho_L}{3\pi} \frac{(\pi/2 - \varepsilon)\cos\varepsilon + \sin\varepsilon}{\cos\theta_i + \cos\theta_v}(1-\Delta) + \rho_0\Delta \tag{5}$$

where

$$\Delta = e^{-[0.5LAI(\sec\theta_i + \sec\theta_v)]} \tag{6}$$

where ρ_0, is the average (assumed) Lambertian reflectance of the layer beneath the thin topmost part of the canopy, ρ_L is the (assumed) Lambertian reflectance of scattering facets – leaves, non-photosynthetic vegetation (litter and woody plant parts) – and *LAI* is the product of facet volume density and area measured for the full height of the canopy. This function is incorporated into the model by assuming a rather lower average reflectance for the understorey directly underneath shrub crowns ($\rho_0 = 0.05$) than for sunlit and viewed background, represented in the model by the calibrated Walthall BRDF model (range 0.23–0.29). Note that the relative contributions of the geometrical and volume scattering phenomena are quite different in magnitude in this semi-arid environment where *LAI* is very low and often <1.0: *LAI* was found to make a difference of only 1–2% in reflectances predicted over the range of angles of the MAO.

The SGM has been previously validated through comparisons with reflectance datasets at a wide range of zenith and azimuth angles – for the set of angular configurations defined by increments in relative azimuth angle of 30° and viewing zenith angle of 15° and at three sun zenith angles, $n = 186$ – calculated with the RGM (Chopping *et al.* 2003). Its adjustable parameters (mean plant density, mean plant radius, *b/r*) were set using field measurements; *h/b*, *LAI* and the 650 nm reflectance of understorey directly underneath shrub crowns were set to fixed values. The R^2 obtained between RGM and SGM were 0.90 and 0.91 for plots 107 and 108, respectively, with little bias. Here, the SGM was also subjected to a series of sensitivity tests by varying one parameter at a time over a typical range of values. Sensitivity to all parameters except *LAI* was effected because in this environment *LAI* is very low and makes very little difference to modelled reflectances (<2%). All parameters except the one being tested were set to fixed values obtained from field survey: for the sparse and dense plots then mean radius (m) was set to 0.230 and 0.168; mean height (m) to 0.337 and 0.234; mean *b/r* ratio to 0.863 and 0.765; and plant density (m^{-2}) to 0.661 and 1.093, respectively.

4. Results and discussion

The RGM runs produced images of the two plots with nadir viewing at all three sun angles (figures 5 and 6), as well as the proportions of all sunlit and shaded components. The bidirectional reflectances calculated from these proportions were in good agreement with the output from the SGM ($R^2 = 0.98$; absolute rms. error = 0.01). The match with the MAO was somewhat less accurate but still good in terms of shape and magnitude ($R^2 = 0.91$–0.93; absolute rms. error = 0.02–0.04). Figure 7 shows the modelling results for the two measured 25 m^2 plots with sparse and dense snakeweed-dominated understoreys at the MAO angles. For these plots the density of the snakeweed understorey is 0.61 m^{-2} (382 plants per 25 m^2) and 1.06 m^{-2} (660 plants per 25 m^2), respectively. Note that the Y-axis scale in these plots ranges from 0.10 to 0.30 reflectance (dimensionless). The soil BRDF shape derived from the Walthall model calibrated with ground goniometer BRDF samples is also shown. The RGM and SGM outputs are very similar in view of the different methods used to calculate the reflectance response of these two contrasting plots.

Tests on the SGM show that it is very sensitive to the input parameters (mean

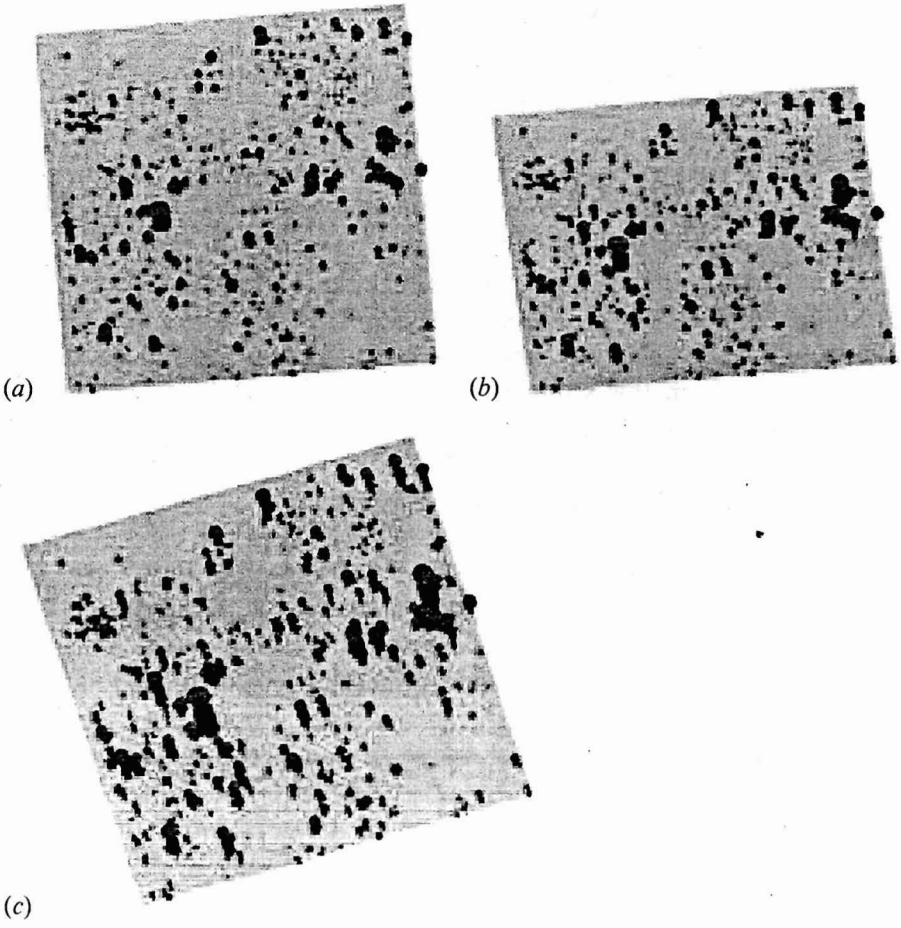

Figure 5. Oblique views of plot 107 (sparse snakeweed; 25 m^2) generated by the RGM. Green features are vegetation (mostly shrubs), dark features are shaded vegetation and soil; the sunlit soil background is in tan. (*a*) SZA 38°, VZA 14°, RAA 175°; (*b*) SZA 49°, VZA 40°, RAA 174°; (*c*) SZA 59°, VZA 24°, RAA 163°.

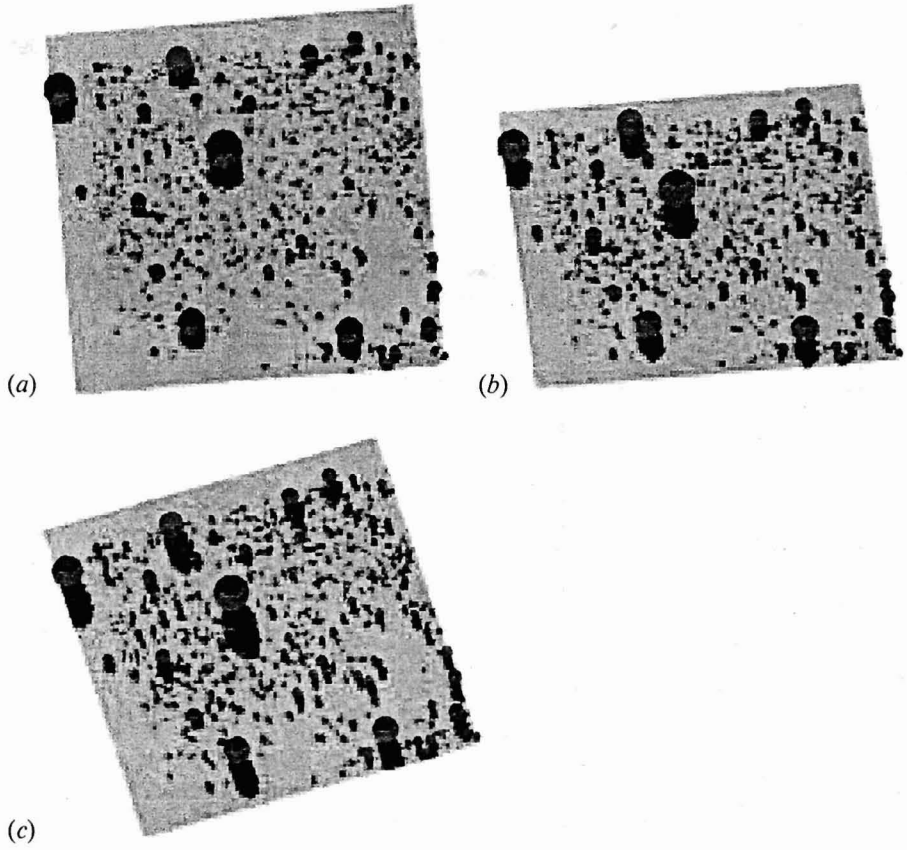

Figure 6. Oblique views of plot 108 (dense snakeweed; 25 m^2) generated by the RGM. Green features are vegetation (mostly shrubs), dark features are shaded vegetation and soil; the sunlit soil background is in tan. Angles as for figure 5.

plant radius, number density, crown height and shape) and so the result is, therefore, not obviously spurious. Sensitivity to plant number density is shown in figure 8; for each of the VZA (view zenith angle) series, reflectance was decreased by a factor of at least 1.44 by changing mean plant number density from 0.0 to 1.1 plants m^{-2}. A wider range of reflectance values was produced at higher solar zenith angles than at lower solar zenith angles. At zero plant number density, the model response is identical to the Walthall soil BRDF. Similarly, sensitivity to plant radius, mean *h*/*b* ratio and mean *b*/*r* ratio is high (figures 9–11), with large changes in the outputs as a result of varying these input parameters over the ranges typically encountered. The model is least sensitive to the *h*/*b* ratio, a measure of crown height, implying that fixing this parameter is indicated for inversion attempts (cf. Abuelgasim *et al.* 1998, Chopping *et al.* 2003).

The RGM modelling results for the same plots are also shown with snakeweed 'removed', i.e. the proportions of sunlit and shaded snakeweed and soil shaded by snakeweed reassigned to sunlit soil (figure 7). Snakeweed accounts for >99% of all understorey plants by number and tends to be associated here with a remnant grama grass cover, especially in the dense plot. In both cases the reassignment made an important difference with a much larger impact in the dense case, as expected (figure 12). In the sparse understorey case, there were increases in modelled

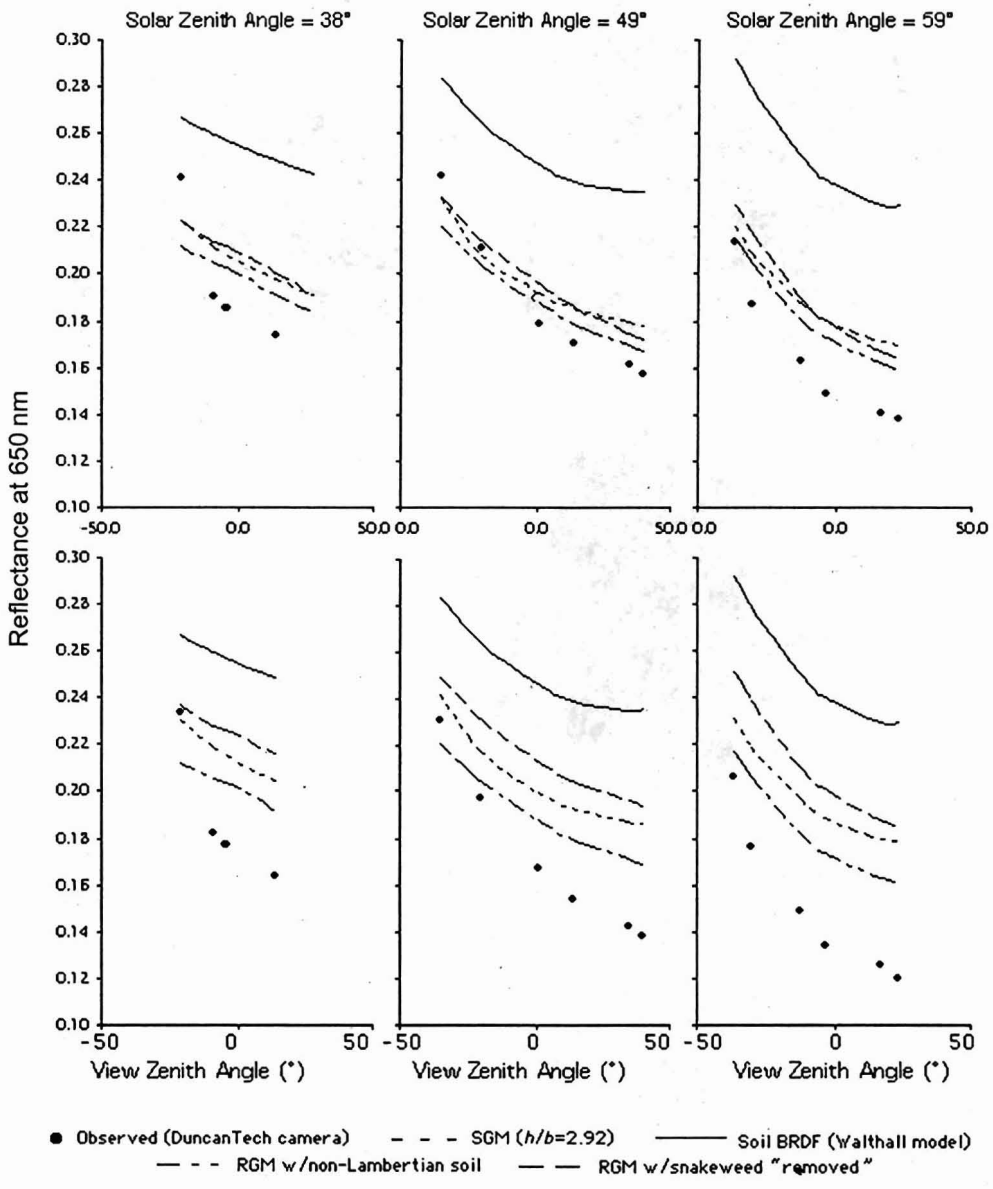

Figure 7. SGM, RGM and MAO (25 m^2 plots close to the PP). Top row: sparse understorey (plot 107); bottom row: dense understorey (plot 108). Also shown are the soil BRDF function (Walthall model) and RGM with snakeweed 'removed' (the proportions of sunlit and shaded snakeweed and soil shaded by snakeweed reassigned to sunlit soil).

reflectance in the range 2.8–6.4% (mean = 4.5%), over all view and sun zenith angles, while in the dense understorey case the range was 11.2–16.0% (mean = 13.7%). This shows that the understorey cannot be neglected in reflectance modelling, which is also qualitatively evident from aerial photography (figure 1(*b, c*)).

The analysis presented here indicates that the presence of snakeweed is unlikely to be the sole cause of divergence between modelled and observed DuncanTech camera reflectance profiles. The most plausible explanation is the presence of sparse grama grass and grass litter. These components were not included in the modelling – because they are not mappable as discrete objects – but are evidently important. This argument is supported by field observations and by the fact that the divergence

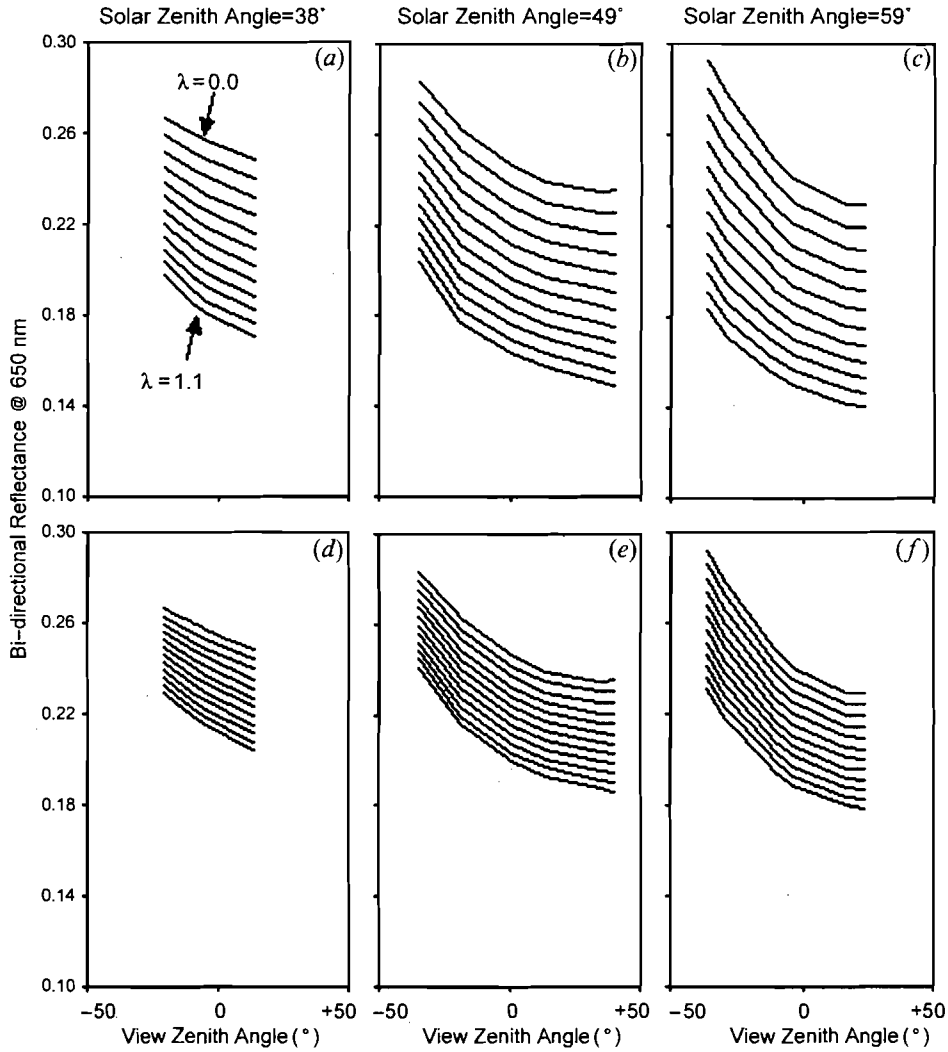

Figure 8. Sensitivity of the SGM to mean plant number density at three solar zenith angles (*a*)–(*c*) plot 107, (*d*)–(*f*) plot 108. Mean plant density was varied from 0.0–1.1 plants m^{-2} providing a sequence with the uppermost series corresponding to density = 0 (i.e. 'no plants', equivalent to the soil BRDF function) and the lowermost series corresponding to density = 1.1.

becomes greater from the backward to forward-scattering viewing directions: this implies greater shadowing of soil indicating that protrusions from the surface must be greater in number or size if the RGM and SGM modelling is to match the observations. Parameterizing the effects of the grass and litter components thus presents a problem for modelling. A potential solution would be to lower the bulk spectral reflectance value assigned to areas with a high snakeweed density. However, the utility of this approach would depend on the validity of the assumption that in these transition zones grama grass abundance is higher in areas where snakeweed is also abundant. Unfortunately, this assumption does not seem to be supportable and other means of assessing understorey density or brightness *a priori* must be sought.

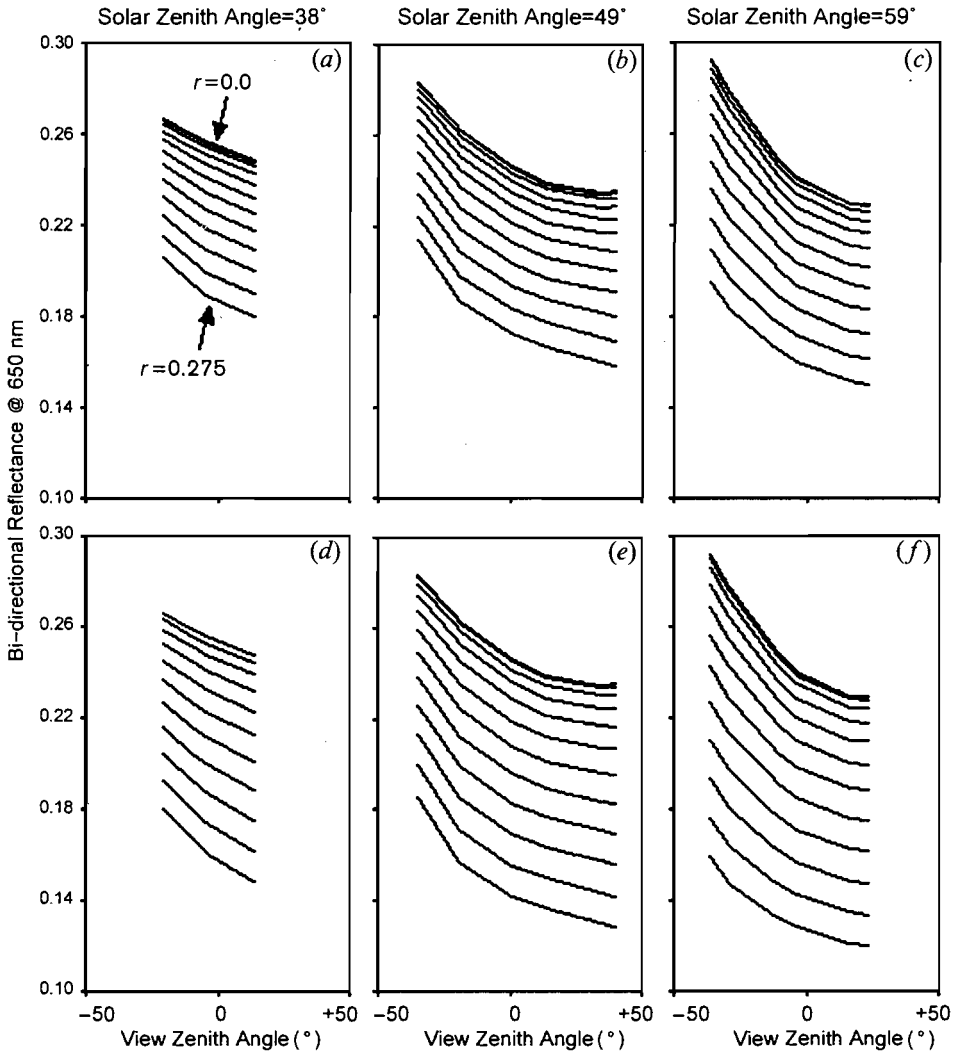

Figure 9. Sensitivity of the SGM to mean plant radius at three solar zenith angles (*a*)–(*c*) plot 107, (*d*)–(*f*) plot 108. Mean plant radius was varied from 0.0–0.275 m providing a sequence with the uppermost series corresponding to radius = 0 (i.e. 'no plants', equivalent to the soil BRDF function) and the lowermost series corresponding to radius = 0.275 m.

5. Conclusions

Chihuahuan Desert grass–shrub transition landscapes present important challenges for BRDF modelling and physical remote sensing. Although soil is the most important component governing brightness and anisotropy with a fractional cover often >0.7, the presence of both the understorey of small forbs and sub-shrubs such as broom snakeweed and black grama grass and its litter play an important role in relation to that of the overstorey of larger shrubs such as honey mesquite, Mormon tea and soaptree yucca. Assigning the understorey proportions to soil (i.e. 'removing' snakeweed) has an important impact especially where density is high, increasing bidirectional reflectance by up to 14% in the two plots surveyed here. There is clearly the possibility of a higher impact in areas where snakeweed density is higher, such as to the immediate NE of the study area (figure 1(*b*)). The root causes of the discrepancies between the modelled values and

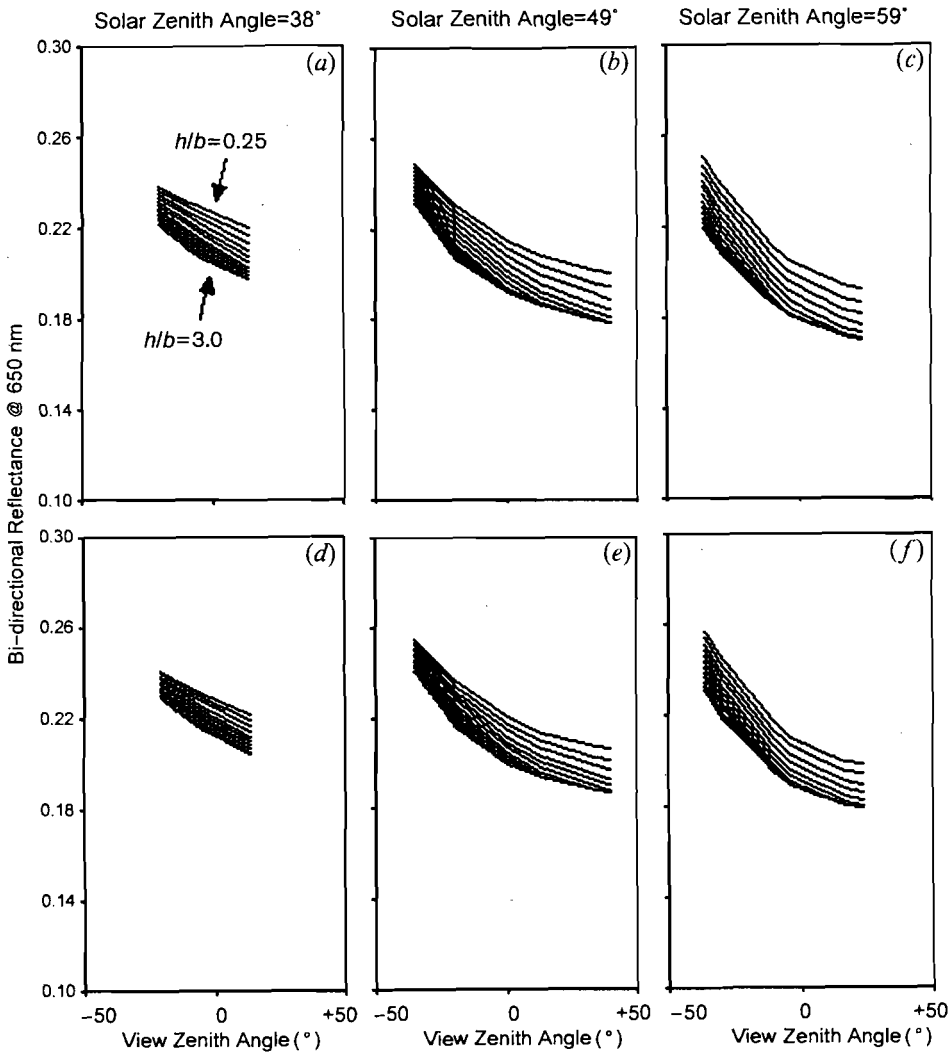

Figure 10. Sensitivity of the SGM to mean *h/b* ratio (height of crown centre/vertical crown radius) at three solar zenith angles (*a*)–(*c*) plot 107, (*d*)–(*f*) plot 108. Mean *h/b* ratio was varied from 0.25–3.0 providing a sequence with the upper (lower) series corresponding to lower (higher) values.

the MAO are not easy to determine. The most plausible explanation is a higher proportion of grama grass and its litter, since the larger disparities occur in the forward-scattering direction. The most likely phenomenon behind this effect is additional shadowing not accounted for in the modelling, probably owing to remnant grama grass and grass litter. Therefore, to be accurate models must not only include a non-Lambertian soil and account for any understorey of small plants but must also account for grass and litter components. This remains a problem for both forward and inverse modelling; a potential solution might be observations with a high resolution instrument sampling the background sparsely. The simulations show that a simplified geometric-optics model closely follows the bidirectional reflectance values predicted by the RGM 3D model and provides a reasonable match with MAO, with maximum absolute rms. error of 0.039 and 0.015 and minimum R^2 of 0.91 and 0.98 with respect to the MAO and RGM,

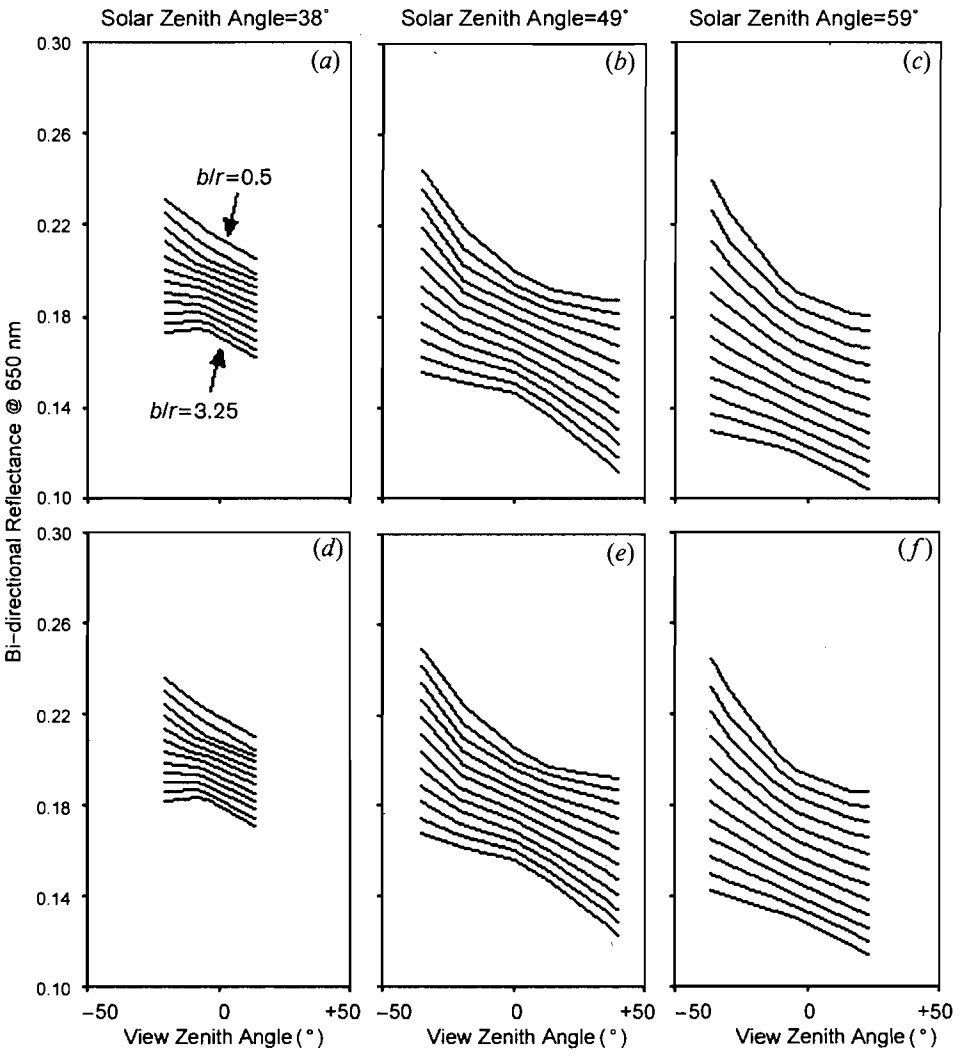

Figure 11. Sensitivity of the SGM to mean *b/r* ratio (vertical to horizontal crown radius) at three solar zenith angles (*a*)–(*c*) plot 107, (*d*)–(*f*) plot 108. Mean *b/r* ratio was varied from 0.5–3.25 providing a sequence with the upper (lower) series corresponding to lower (higher) values.

respectively. Sensitivity tests showed that the SGM is very sensitive to input parameters, indicating that these results are not spurious.

Acknowledgments

A portion of the work presented here was accomplished while the principal author was a post-doctoral fellow with the USDA, ARS Jornada Experimental Range. The authors gratefully acknowledge the assistance of Christoph Borel at Los Alamos National Laboratory, Los Alamos, NM; the staff of the USDA, ARS Jornada Experimental Range, Las Cruces, NM and, in particular, Kris Havstad, Eddie Garcia, Jim Lenz, Dave Thatcher and Rob Dunlap; Betty Walter-Shea at the School of Natural Resource Sciences at the University of Nebraska-Lincoln; Wenhan Qin at Science Systems and Applications, Inc., Lanham, MD; and Rob Parry at the Hydrology and Remote Sensing Laboratory, Beltsville, MD.

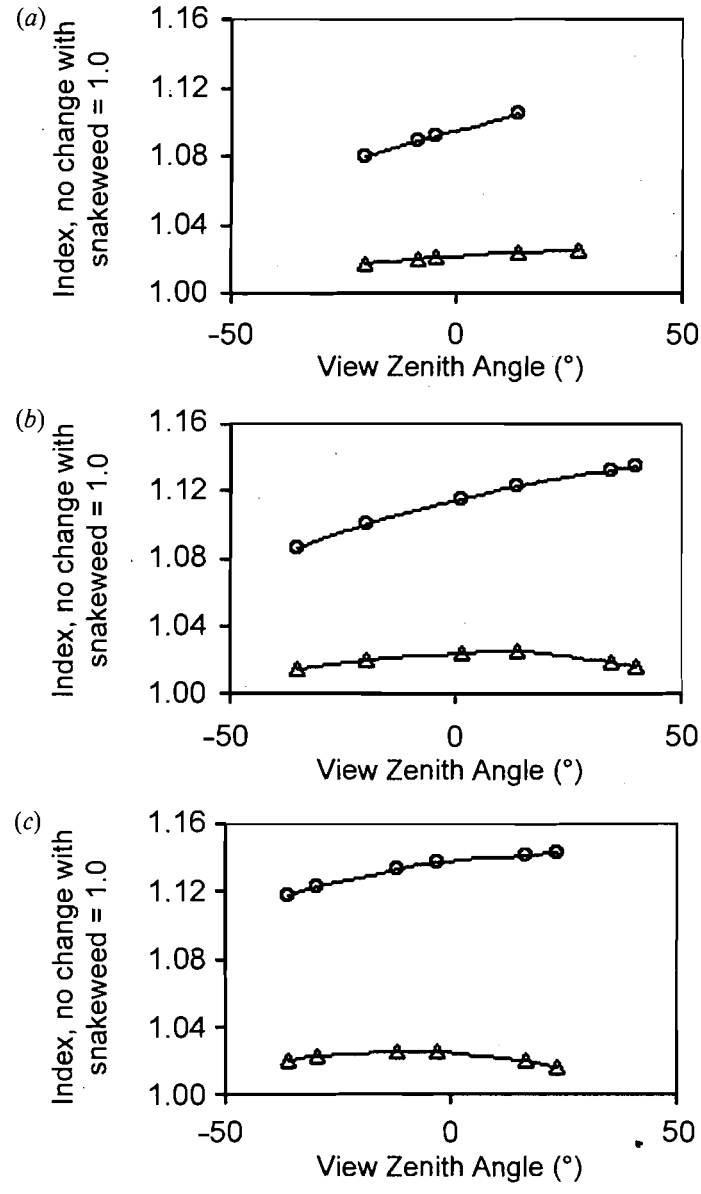

Figure 12. The impact of removing the snakeweed understorey on modelled BRFs, Index, with snakeweed = 1.0. (*a*) SZA = 38°; (*b*) SZA = 49; (*c*) SZA = 59°. Triangles: plot 107 (sparse snakeweed: 0.61 m^{-2}); circles: plot 108 (dense snakeweed: 1.06 m^{-2}).

References

ABUELGASIM, A. A., GOPAL, S., and STRAHLER, A. H., 1998, Forward and inverse modelling of canopy directional reflectance using a neural network. *International Journal of Remote Sensing*, **19**, 453–471.

ARCHER, S., BOUTTON, T. W., and HIBBARD, K. A., 2001, Trees in grasslands: biogeochemical consequences of woody plant expansion: Global biogeochemical cycles in the climate system. In *Global Biogeochemical Cycles in the Climate System*, edited by Ernst-D. Schulze, S. P. Harrison, M. Heimann, E. A. Holland, J. Lloyd, I. C. Prentice and D. Schimel (San Diego: Academic Press), pp. 115–137.

ASNER, G. P., BATESON, C. A., TOWNSEND, A. R., and WESSMAN, C. A., 1999, Resolving vegetation condition and biogeochemical processes using hyperspectral-BRDF

inverse modeling. *Proceedings of the Eighth Annual JPL Airborne Earth Science Workshop* (Pasadena: NASA Jet Propulsion Laboratory), pp. 37–46.

ASNER, G. P., WESSMAN, C. A., BATESON, C. A., and PRIVETTE, J. L., 2000, Impact of tissue, canopy, and landscape factors on the hyperspectral reflectance variability of arid ecosystems. *Remote Sensing of Environment*, **74**, 69–84.

BUFFINGTON, L. C., and HERBEL, C. H., 1965, Vegetational changes on a semidesert grassland range from 1858 to 1963. *Ecological Monographs*, **35**, 139–164.

CHOPPING, M. J., RANGO, A., HAVSTAD, K. M., SCHIEBE, F. R., RITCHIE, J. C., SCHMUGGE, T. J., FRENCH, A., SU, L., MCKEE, L., and DAVIS, M. R., 2003, Canopy attributes of Chihuahuan Desert grassland and transition communities derived from multi-angular airborne imagery. *Remote Sensing of Environment*, **85**, 339–354.

EVERITT, J. H., ALANIZ, M. A., DAVIS, M. R., ESCOBAR, D. E., HAVSTAD, K. M., and RITCHIE, J. C., 1997, Light reflectance characteristics and video remote sensing of two range sites on the Jornada Experimental Range. *Proceedings of the 16th Biennial Workshop on Videography and Color Photography in Resource Assessment* (Bethesda: ASPRS), pp. 485–495.

FRIEDEL, M. H., 1991, Range condition assessment and the concept of thresholds: a viewpoint. *Journal of Range Management*, **44**, 422–426.

GIBBENS, R. P., BECK, R. F., MCNEELY, R. P., and HERBEL, C. H., 1992, Recent rates of mesquite establishment in the northern Chihuahuan Desert. *Journal of Range Management*, **45**, 585–588.

GOEL, N. S., 1988, Models of vegetation canopy reflectance and their use in estimation of biophysical parameters from reflectance data. *Remote Sensing Reviews*, **4**, 1–21.

HALL, F., TOWNSHEND, J. R. G., and ENGMAN, E., 1995, Status of remote sensing algorithms for estimation of land surface state parameters. *Remote Sensing of Environment*, **51**, 138–156.

HUENNEKE, L. F., ANDERSON, J. P., REMMENGA, M., and SCHLESINGER, W. H., 2002, Desertification alters patterns of aboveground net primary production in Chihuahuan ecosystems. *Global Change Biology*, **8**, 247–264.

LI, X., and STRAHLER, A. H., 1992, Geometric-optical bidirectional reflectance modeling of the discrete crown vegetation canopy: effect of crown shape and mutual shadowing. *IEEE Transactions on Geoscience and Remote Sensing*, **30**, 276–291.

NI, W., and LI, X., 2000, A coupled vegetation–soil bidirectional reflectance model for a semi-arid landscape. *Remote Sensing of Environment*, **74**, 113–124.

PELGRUM, H., SCHMUGGE, T., RANGO, A., RITCHIE, J., and KUSTAS, W., 2000, Length scale analysis of surface albedo, temperature and NDVI in a desert grassland. *Water Resources Research*, **36**, 1757–1765.

QIN, W., and GERSTL, S. A. W., 2000, 3-D scene modeling of Jornada semi-desert vegetation cover and its radiation regime. *Remote Sensing of Environment*, **74**, 145–162.

RITCHIE, J. C., RANGO, A., KUSTAS, W. P., SCHMUGGE, T. J., BRUBAKER, K., HAVSTAD, K. M., NOLEN, B., PRUEGER, J. H., EVERITT, J. H., DAVIS, M. R., SCHIEBE, F. R., ROSS, J. D., HUMES, K. S., HIPPS, L. E., MENENTI, M., BASTIAANSSEN, W. G. M., and PELGRUM, H., 1996, JORNEX: An airborne campaign to quantify rangeland vegetation change and plant community-atmospheric interactions. *Proceedings of the Second International Airborne Remote Sensing Conference and Exhibition* (San Francisco: ERIM), pp. II-55–I–66.

ROSS, J. K., 1981, *The Radiation Regime and Architecture of Plant Stands* (The Hague: Dr W. Junk Publishers).

ROUJEAN, J.-L., LEROY, M., and DESCHAMPS, P.-Y., 1992, A bidirectional reflectance model of the Earth's surface for the correction of remote sensing data. *Journal of Geophysical Research*, **97**, 20 455–20 468.

SCHLESINGER, W. H., REYNOLDS, J. F., CUNNINGHAM, G. L., HUENNEKE, L. F., JARRELL, W. M., VIRGINIA, R. A., and WHITFORD, W. G., 1990, Biological feedbacks in global desertification. *Science*, **247**, 1043–1048.

SMITH, S. D., HUXMAN, T. E., ZITZER, S. F., CHARLET, T. N., HOUSMAN, D. C., COLEMAN, J. S., FENSTERMAKER, L. K., SEEMANN, J. R., and NOWAK, R. S., 2000, Elevated CO_2 increases productivity and invasive species success in an arid ecosystem. *Nature*, **408**, 79–82.

VERMOTE, E., TANRE, D., DEUZE, J. L., HERMAN, M., and MORCRETTE, J. J., 1997, Second

Simulation of the Satellite Signal in the Solar Spectrum, (6S): an overview. *IEEE Transactions on Geoscience and Remote Sensing*, **35**, 675–686.

VERSTRAETE, M. M., PINTY, B., and DICKINSON, R. E., 1990, A physical model of the bidirectional reflectance of vegetation canopies, 1. Theory. *Journal of Geophysical Research*, **95**, 11 755–11 765.

WALTHALL, C. L., NORMAN, J. M., WELLES, J. M., CAMPBELL, G., and BLAD, B. L., 1985, Simple equation to approximate the bidirectional reflectance from vegetative canopies and bare surfaces. *Applied Optics*, **24**, 383–387.

WANNER, W., LI, X., and STRAHLER, A. H., 1995, On the derivation of kernels for kernel-driven models of bidirectional reflectance. *Journal of Geophysical Research*, **100**, 21 077–21 090.

WERNECKE, P., BUCK-SORLIN, G. H., and DIEPENBROCK, W., 2000, Combining process–with architectural models: The simulation tool VICA. *Systems–Analysis–Modelling–Simulation* **39**, 235–277, http://www.landw.uni-halle.de/aoei/vica_1.PDF [accessed 4 September 2002].

WHITE, M. A., ASNER, G. P., NEMANI, R. R., PRIVETTE, J. L., and RUNNING, S. W., 2000, Measuring fractional cover and leaf area index in arid ecosystems – digital camera, radiation transmittance, and laser altimetry methods. *Remote Sensing of Environment*, **74**, 45–57.